HOKKAIDO UNIVERSITY

Title	Impacts of hexadecapole correlations in actinide nuclei
Author(s)	Lotina, L.; Nomura, K.; Rodriguez-Guzman, R. et al.
Citation	Physical Review C, 114(1) https://doi.org/10.1103/n5xp-fntr
Issue Date	2026-07-27
Doc URL	https://hdl.handle.net/2115/100318
Rights	©2026 American Physical Society
Type	journal article
File Information	v6.pdf

Hokkaido University Collection of Scholarly and Academic Papers : HUSCAP

Impacts of hexadecapole correlations in actinide nuclei

L. Lotina,[1,*] K. Nomura,[2,3,†] R. Rodríguez-Guzmán,[4,‡] and L. M. Robledo[5,6]

[1] *Division of Radiation Protection, Institute for Medical Research and Occupational Health, HR-10000 Zagreb, Croatia*
[2] *Department of Physics, Hokkaido University, Sapporo 060-0810, Japan*
[3] *Nuclear Reaction Data Center, Hokkaido University, Sapporo 060-0810, Japan*
[4] *Department of Physics, School of Sciencies and Humanities, Nazarbayev University, 53 Kabanbay Batyr Ave., Astana 010000, Kazakhstan*
[5] *Departamento de Física Teórica and CIAFF, Universidad Autónoma de Madrid, E-28049 Madrid, Spain*
[6] *Center for Computational Simulation, Universidad Politécnica de Madrid, Campus de Montegancedo, Bohadilla del Monte, E-28660-Madrid, Spain*

(Dated: July 10, 2026)

The impact of hexadecapole correlations on the low-energy spectroscopic properties of Th, U, and Pu nuclei, within the mass range $232 \leq A \leq 240$, is studied systematically using the mapped *sdg*-IBM model. Fermionic input is obtained via the quadrupole-hexadecapole constrained Hartree-Fock-Bogoliubov approximation, based on the parametrization D1S of the Gogny energy density functional. The *sdg*-IBM Hamiltonian parameters are determined by mapping the quadrupole-hexadecapole fermionic mean-field potential energy surfaces onto the corresponding bosonic surfaces. The low-energy spectra and transition strengths, obtained via the diagonalization of the *sdg*-IBM Hamiltonian, compare well with the available experimental data. It is shown that the effects of hexadecapole collectivity can be observed in high-spin yrast states with spins $J^\pi \geqslant 10^+$. The mapped *sdg*-IBM improves the excitation energies of those states, as compared with the simpler *sd*-IBM model. The *sdg*-IBM also improves the description of the $E2$ transition strengths between high-spin yrast states and predicts strong $E4$ transitions from nonyrast 4^+ states to the 0^+ ground state.

I. INTRODUCTION

Intrinsic deformations represent a prominent aspect of atomic nuclei with an impact on several nuclear structure properties [1]. Within this context, the most common intrinsic deformation is of quadrupole type. Such quadrupole deformations have been extensively studied and their fingerprints on the low-energy positive-parity states are well known. On the other hand, the (second-order) hexadecapole deformations also contribute to the positive-parity states [1]. However, as both the quadrupole and hexadecapole deformations affect states with the same parity quantum numbers, the dominant quadrupole correlations often overshadow the hexadecapole correlation effects. Nevertheless, hexadecapole correlations have already been observed in different regions of the nuclear chart such as the light [2], medium-heavy [3], rare-earth [4, 5], transitional metals [6, 7], and actinide [8, 9] regions. The $K^\pi = 4^+$ bands at low energy, which exhibit pronounced $E4$ transitions to the ground-state band, provide characteristic observables associated with hexadecapole correlations. Recently, a significant interest has been devoted to studying the hexadecapole deformation effects in relativistic heavy ion collisions of actinide nuclei, especially in ^{238}U [10–12]. It is therefore timely and relevant to conduct a systematic theoretical study of hexadecapole deformation effects in actinide nuclei using a microscopic model.

One of the most commonly employed models to describe collective properties in nuclei is the interacting boson model (IBM) [13]. In the simplest version of the IBM, called the *sd*-IBM, a nucleus is approximated as a system composed of an inert core, defined by the nearest double-magic nucleus, and valence nucleons that couple into the correlated monopole (with spin and parity 0^+) and quadrupole (2^+) pairs, which are represented by s and d bosons, respectively [14, 15]. The interactions between those bosons give rise to the low-energy quadrupole collective states. The hexadecapole degree of freedom is introduced in the IBM via the inclusion of g bosons (4^+), corresponding to the hexadecapole pairs of valence nucleons. This extension is called the *sdg*-IBM, and it has already been used in previous studies [16–23].

Originally, the IBM was built as a phenomenological model and the parameters of the IBM Hamiltonian had to be fitted to experimental data corresponding to the low-lying energy spectrum for each nucleus. In the last decades a fermion-to-boson mapping procedure has been developed [24, 25] that allows to derive the parameters of the IBM Hamiltonian microscopically, i.e., by fitting them to the potential energy surface (PES) obtained within the constrained self-consistent mean-field (SCMF) approximation, based on a given universal energy density functional (EDF) [26–28]. The fermion-to-boson mapping procedure has been successfully employed to describe the effects of axial and triaxial quadrupole [24, 29–31] as well as octupole [32–34] correlations in atomic nuclei. The mapped IBM has also been employed in the analysis of hexadecapole correlations in rare-earth nuclei [35–37]. For a detailed account of the fermion-to-boson mapping procedure the reader is referred to Ref. [25] and

* llotina@imi.hr
† nomura@sci.hokudai.ac.jp
‡ guzman.rodriguez@nu.edu.kz

references therein.

In this work, we extend the analyses of the quadrupole-hexadecapole mapping procedure, already carried out for rare-earth nuclei [35–37], to the actinide region of the nuclear chart. To this end, we have considered the isotopic chains $^{232-240}$Th ($Z = 90$), $^{232-240}$U ($Z = 92$), and $^{232-240}$Pu ($Z = 94$). As an input, we have considered the Hartree-Fock-Bogoliubov (HFB) approximation, based on the Gogny-D1S [38, 39] EDF. This microscopic mean field framework has been extensively applied to nuclei across the whole nuclear chart [28, 40]. It has also been successfully combined with the IBM mapping procedure already mentioned above to analyze the impact of the quadrupole [30, 41–44], and octupole [45–49] correlations on the spectroscopic properties of even-even nuclei.

The quadrupole-hexadecapole coupling has been studied recently at the HFB level with the help of constrains on the (axial) quadrupole and hexadecapole operators in Sm, Gd, rare-earth and actinide nuclei [50–52]. Those previous studies [50–52] have also considered the role of the zero-point quantum quadrupole-hexadecapole fluctuations within the framework of the two-dimensional (2D) Generator Coordinate Method (GCM) [26, 28, 53, 54]. Both at the HFB and 2D-GCM levels, calculations have been carried out in terms of the Gogny-D1S EDF. In this paper, we will consider an alternative and more detailed description of spectroscopic properties along the selected Th, U and Pu isotopic chains. In particular, we examine the role of the hexadecapole degree of freedom in the low-lying states of the selected set of even-even Th, U and Pu nuclei within the framework of the Gogny-D1S HFB mapped *sdg*-IBM model. To better undertand the role of hexadecapole correlations, comparisons will be presented with results obtained within the Gogny-D1S HFB mapped *sd*-IBM model.

It is worth mentioning that the considered nuclei have been shown to exhibit some degree of octupole collectivity [55, 56] which in turn might have certain influence on the positive-parity states, such as the excited 0^+ states [33, 46, 57, 58]. In this study, we neglect such octupole correlation effects not only for the sake of simplicity, but also because the octupole degree of freedom is more relevant for the properties of negative-parity states.

The paper is organized as follows. The theoretical framework used is briefly outlined in Sec. II. Such a theoretical scheme comprises the Gogny-D1S SCMF calculations as well as the mapped *sdg*-IBM and *sd*-IBM. The (axial) quadrupole-hexadecapole PESs obtained from the SCMF and IBM calculations are discussed in Sec. III. The results of the spectroscopic calculations are presented in Sec. IV. Finally, Sec. V is devoted to the concluding remarks and work perspectives.

II. MODEL DESCRIPTION

For the selected set of Th, U and Pu nuclei, the SCMF PESs are obtained within the constrained Gogny-D1S HFB approximation [38, 39]. Constrains on the (axial) quadrupole $\hat{Q}_{20}$ and hexadecapole $\hat{Q}_{40}$ operators are used to explore the PES for the two degrees of freedom. It is convenient to use mass independent deformation parameters $\beta_{\lambda 0}$ ($\lambda = 2, 4$) which are defined in the standard way as [50–52]

$$\beta_{\lambda 0} = \frac{\sqrt{4\pi(2\lambda+1)}}{3R^{\lambda}A} \langle \hat{Q}_{\lambda 0} \rangle \ , \tag{1}$$

where $R = 1.2A^{1/3}$ fm is the radius and A is the mass number. For simplicity, we denote $\beta_{\lambda 0}$ as β_{λ}, since axial symmetry is kept as a self-consistent symmetry in the Gogny-HFB calculations. In Eq.(1), $\langle \hat{Q}_{\lambda 0} \rangle$ represents the average value of quadrupole and/or hexadecapole multipole operator in the corresponding HFB state. More details on the (β_2, β_4)-constrained Gogny-HFB calculations can be found in Ref. [51].

In order to obtain low-energy spectra and transition properties, calculations have been carried out within the (mapped) *sdg*-IBM. For the *sdg*-IBM model Hamiltonian, we have assumed the same form as in previous studies [35–37]:

$$\hat{H} = \epsilon_d \hat{n}_d + \epsilon_g \hat{n}_g + \kappa \hat{Q}^{(2)} \cdot \hat{Q}^{(2)} + \kappa(1-\chi^2)\hat{Q}^{(4)} \cdot \hat{Q}^{(4)}. \tag{2}$$

where $\hat{n}_d = d^{\dagger} \cdot \tilde{d}$ and $\hat{n}_g = g^{\dagger} \cdot \tilde{g}$ represent the d- and g-boson number operators, respectively, while

$$\hat{Q}^{(2)} = (s^{\dagger} \times \tilde{d} + d^{\dagger} \times s) + \chi \left[\frac{11\sqrt{10}}{28} (d^{\dagger} \times \tilde{d})^{(2)} - \frac{9}{7}\sigma (d^{\dagger} \times \tilde{g} + g^{\dagger} \times \tilde{d})^{(2)} + \frac{3\sqrt{55}}{14} (g^{\dagger} \times \tilde{g})^{(2)} \right], \tag{3}$$

and

$$\hat{Q}^{(4)} = s^{\dagger} \times \tilde{g} + g^{\dagger} \times s \tag{4}$$

stand for the boson image of the quadrupole and hexadecapole operators, respectively. In principle, the *sdg*-boson model Hamiltonian should include more interaction terms and the corresponding parameters [13]. However, as already shown in previous studies [35–37], the Hamiltonian Eq.(2) provides a reasonable starting point to describe the properties of nuclei for which the experimental data suggest a pronounced quadrupole-hexadecapole coupling. It also satisfies the U(5) $\otimes$ U(9), SU(3) and O(15) dynamical symmetries [23, 59]. For $\sigma = 1$, the Hamiltonian Eq.(2) is equivalent to the one considered in Ref. [23]. In order to guarantee the physical meaning of each term of the *sdg*-IBM Hamiltonian, it is assumed that the quadrupole interaction is attractive ($\kappa < 0$) and that the energy required for two valence nucleons to couple into a d-boson is smaller than the energy required for them to couple into a g-boson ($\epsilon_d < \epsilon_g$). Furthermore, as the considered actinide nuclei display strong axial deformations, they are assumed to be close to the SU(3) limit of the *sdg*-IBM. To meet

the requirement for the Hamiltonian to be in the SU(3) symmetry limit, the parameters λ and σ must satisfy the conditions $-1 \leqslant \chi \leqslant +1$ and $-1 \leqslant \chi\sigma \leqslant +1$ [23].

The parameters ϵ_d, ϵ_g, κ, χ and σ are determined using the *sdg*-IBM mapping procedure developed in Ref. [35]. To connect the *sdg*-IBM to the geometric model of the nucleus [60, 61], a coherent state (up to the normalization factor)

$$|\phi\rangle = (1 + \tilde{\beta}_2 d_0^\dagger + \tilde{\beta}_4 g_0^\dagger)^{N_B} |0\rangle \ , \tag{5}$$

is introduced, where N_B and $|0\rangle$ represent the number of bosons and the boson vacuum (or the inert core). On the other hand, $\tilde{\beta}_2$ and $\tilde{\beta}_4$ are the axial bosonic quadrupole and hexadecapole deformations, which, as shown below, are related to the fermionic deformations of Eq. (1). For all the considered isotopes, the inert core corresponds to the doubly-magic nucleus $^{208}_{82}$Pb, while the number of bosons is equal to $N_B = 12 - 16$ for the even-even nuclei with $A = 232 - 240$. The *sdg*-IBM PES, as a function of the $\tilde{\beta}_2$ and $\tilde{\beta}_4$ deformations, is obtained as the expectation value of the Hamiltonian (2) in the coherent state $\langle\phi\rangle$ (5), i.e., $E_{\rm IBM}(\tilde{\beta}_2, \tilde{\beta}_4) = \langle\phi| \hat{H} |\phi\rangle / \langle\phi|\phi\rangle$. The exact analytical form of the *sdg*-IBM PES can be found in Refs. [21, 23].

The parameters of the *sdg*-IBM are determined so that the bosonic PES, $E_{\rm IBM}(\tilde{\beta}_2, \tilde{\beta}_4)$, matches as close as possible the Gogny-D1S HFB PES, $E_{\rm SCMF}(\beta_2, \beta_4)$, near the absolute minimum:

$$E_{\rm SCMF}(\beta_2, \beta_4) \approx E_{\rm IBM}(\tilde{\beta}_2, \tilde{\beta}_4) \ . \tag{6}$$

The standard assumption of the IBM mapping procedure is that the bosonic axial deformations should be proportional to those of the SCMF calculations, i.e.,

$$\tilde{\beta}_2 = C_2 \beta_2 \quad , \quad \tilde{\beta}_4 = C_4 \beta_4 \ , \tag{7}$$

with C_λ being the proportionality constants. These relations have already been shown to work well in previous calculations including (axial) octupole [32, 33] and hexadecapole [35, 36] deformations. At the end, one should determine seven parameters, 5 in the *sdg*-IBM Hamiltonian, and the two scale factors, C_2 and C_4.

An important point to mention regarding the 2D mapping method with axial deformation parameters as coordinates is that the obtained PESs from the IBM mapping tend to be flat compared to their SCMF counterparts. This is observed both in the case of quadrupole-octupole [32, 33] and quadrupole hexadecapole mapping [35, 36]. This is to be expected, as IBM has a significantly smaller model space than the SCMF models. For the mapping method to be considered successful, certain conditions must be met: first, the positions of the absolute minima of the SCMF PES must be reproduced. Furthermore, IBM PES should also reproduce the overall shape of the SCMF PES as best as possible, and it should also reproduce the existence of low-energy saddle points in the SCMF PES, if there are any. Thirdly, the IBM PES needs to be as close in size as possible to the SCMF counterpart. Finally, all of the parameters must have values consistent with the physical conditions and symmetry limits imposed by the IBM Hamiltonian. Since small variations in the IBM parameters can lead to significant changes in the locations of absolute minima, PES sizes, and saddle point positions, the obtained sets of IBM parameters for each nucleus can be considered to be approximately unique, with possible variations in parameter values being sufficiently small so as not to affect any of the spectroscopic results significantly.

For the *sd*-IBM calculations, the following simple Hamiltonian is employed [13]:

$$\hat{H}_{sd} = \epsilon_d \hat{n}_d + \kappa \hat{Q}^{(2)} \cdot \hat{Q}^{(2)}, \tag{8}$$

with the boson quadrupole operator $\hat{Q}^{(2)}$ being given by

$$\hat{Q}^{(2)} = s^\dagger \tilde{d} + d^\dagger s + \chi (d^\dagger \times \tilde{d})^{(2)}. \tag{9}$$

The parameters ϵ_d, κ, and χ are fitted so that a one-dimensional (1D), *sd*-IBM energy curve should approximately reproduce the Gogny-D1S PES along the $\beta_4 = 0$ line:

$$E_{\rm SCMF}(\beta_2, \beta_4 = 0) \approx E_{sd-{\rm IBM}}(\tilde{\beta}_2) \ . \tag{10}$$

Within the *sd*-IBM mapping, attention is paid to reproduce the positions of the absolute minima, the depth of the potential, and the energy difference between the minimum on the $\beta_4 = 0$ axis and the saddle point on the oblate side of the HFB PES. A similar relationship between the fermionic and bosonic deformations to Eq. (7) is assumed for the *sd*-IBM, that is, $\tilde{\beta}_2 = C_2^{sd} \beta_2$, leaving us with a total of 4 parameters to be determined.

Low-energy spectra and transition strengths have been obtained by diagonalizing the mapped boson Hamiltonians Eqs. (2) and (10). The numerical diagonalization is performed using the computer program ARBMODEL [62].

The bosonic quadrupole $\hat{T}(E2)$ and hexadecapole $\hat{T}(E4)$ transition operators are formulated for both the *sdg*-IBM and *sd*-IBM in the same way as in Refs. [35–37]. The bosonic quadrupole transition operator reads

$$\hat{T}(E2)_{sdg/sd} = e_2^{sdg/sd} \hat{Q}^{(2)}_{sdg/sd}, \tag{11}$$

with $\hat{Q}^{(2)}_{sdg}$ and $\hat{Q}^{(2)}_{sd}$ being the quadrupole operators of the *sdg*-IBM Eq. (3) and *sd*-IBM Eq. (9), with the same values of the parameters χ and σ as those used for these operators. In the *sdg*-IBM, $\hat{T}(E4)_{sdg}$ is given as

$$\hat{T}^{(E4)}_{sdg} = e_4^{sdg} \left[s^\dagger \tilde{g} + g^\dagger s + (d^\dagger \times \tilde{d})^{(4)} \right], \tag{12}$$

while, for the *sd*-IBM, it is of the form:

$$\hat{T}^{(E4)}_{sd} = e_4^{sd} (d^\dagger \times \tilde{d})^{(4)}. \tag{13}$$

The quadrupole effective charge $e_2^{sdg/sd}$ is determined for each nucleus by fitting the calculated quadrupole transition strength, $B(E2; 2_1^+ \rightarrow 0_1^+)$, to the experimental data. Similarly, the hexadecapole effective charge $e_4^{sdg/sd}$ is fitted so that the experimental data on the $B(E4; 4_1^+ \rightarrow 0_1^+)$ transition strength in the yrast band is reproduced. Since data on $E4$ transitions in the actinide region are limited, this calculation is only performed for nuclei for which experimental $B(E4)$ values are available.

III. MAPPING THE SCMF RESULTS ONTO THE IBM SPACE

The Gogny-D1S PESs obtained for even-even Th, U and Pu isotopes with mass number $A = 232 - 236$ are depicted in Fig. 1. Those PESs are shown up to an energy of 2.7 MeV above the HFB ground state. Note, that the PESs for nuclei with $A = 238$ and 240 are not shown in the figure, as they are rather similar to the ones obtained for nuclei with $A = 236$ in each isotopic chain. As can be seen from the figure, all the PESs exhibit a similar topography, i.e., steepness along both the β_2 and β_4 directions as well as the locations of the absolute minima.

In panels (a), (c) and (e) of Fig. 2 we have plotted the quadrupole $\beta_2^{\rm min}$ and hexadecapole $\beta_4^{\rm min}$ deformations corresponding to the absolute minima of the HFB PESs in Fig. 1. In panels (b), (d) and (f) of the same figure, we have also plotted the $\beta_2^{\rm min}$ values along the hexadecapole $\beta_4 = 0$ path.

As can be seen from panels (a), (c) and (e), all the isotopes display pronounced quadrupole $\beta_2^{\rm min} > 0$ deformations [51]. For U and Pu isotopes, the $\beta_2^{\rm min}$ deformations only change slightly with the mass number A, starting with $\beta_2^{\rm min} = 0.26$ at $A = 232$, and increasing up to $\beta_2^{\rm min} = 0.28$ around $A = 240$. In the case of Th isotopes, the largest quadrupole deformation $\beta_2^{\rm min} = 0.28$ corresponds to ^{238}Th, while for ^{240}Th we have obtained the value $\beta_2^{\rm min} = 0.26$.

For the considered Th, U and Pu nuclei, the Gogny-D1S HFB ground states correspond to diamond-like $\beta_4^{\rm min} > 0$ shapes [51]. The $\beta_4^{\rm min}$ values decrease with increasing A. Among the studied isotopic chains, the most pronounced decrease is observed for Th nuclei. On the other hand, for Pu isotopes there is a slight increase from $\beta_4^{\rm min} = 0.18$ in ^{234}Pu to $\beta_4^{\rm min} = 0.2$ in ^{236}Pu, after which the $\beta_4^{\rm min}$ values continue decreasing.

As can be seen from panels (b), (d) and (f), the $\beta_2^{\rm min}$ values along the $\beta_4 = 0$ path in the PESs are smaller than those found in the (β_2, β_4)-constrained HFB calculations [51]. In this case, we have found $\beta_2^{\rm min}$ deformations ranging from $\beta_2^{\rm min} = 0.16$ (^{232}Pu) or 0.18 (^{232}Th and ^{232}U) to $\beta_2^{\rm min} = 0.22$ (^{240}U) or 0.24 (^{240}Th and ^{240}Pu).

The mapped *sdg*-IBM PESs obtained for ^{232,234,236}Th, ^{232,234,236}U and ^{232,234,236}Pu are shown in Fig. 3. From the comparison with the fermionic PESs in Fig. 1, one realizes that the mapping procedure reproduces the location of the absolute minima. Nevertheless, the *sdg*-IBM PESs are flatter than the SCMF ones in the region corresponding to larger β_2 and β_4 deformations. This difference between the mapped IBM and SCMF PESs is a well known feature arising from the different size of the models spaces employed in each of these frameworks. The IBM model considers a given valence space, while all the nucleonic degrees of freedom are incorporated in a much larger fermionic model space within the SCMF scheme.

The *sdg*- and *sd*-IBM parameters, obtained via the mapping procedure, are depicted in Figs. 4 and 5, as functions of the mass number A. In the *sdg*-IBM, the d-boson energy remains nearly constant at $\epsilon_d \approx 0.2 - 0.22$ MeV. This reflects, that the quadrupole deformations $\beta_2^{\rm min}$ do not change significantly with A. In the *sd*-IBM, ϵ_d stays constant at 0.2 MeV for Th and Pu isotopes, while for U isotopes, it slightly increases with A.

Within the *sdg*-IBM, the parameter κ, which is not shown in Fig. 4, is constant ($\kappa = -0.04$ MeV). This is because, for the considered nuclei, the topography of the PESs is similar and the location of the absolute minimum does not differ much from one another. However, within the *sd*-IBM, the parameter κ (see, Fig. 5) is constant for Pu isotopes, while for Th and U nuclei it slightly decreases in magnitude with A.

The χ parameter exhibits a similar behavior in both the mapped *sdg*-IBM and *sd*-IBM models, i.e., it increases its absolute value with A. This reflects the increase of the $\beta_2^{\rm min}$ values. However, the parameter C_2 exhibits a different behavior in the two IBM models. In the case of the *sdg*-IBM, it fluctuates between $C_2 = 5.0$ and 4.5, while it decreases monotonously with A in the *sd*-IBM. This different behavior results from the fact that in the (β_2, β_4)-constrained Gogny-D1S HFB calculations the $\beta_2^{\rm min}$ values slightly increase with A. On the other hand, the quadrupole deformation corresponding to the minimum along the $\beta_4 = 0$ axis increases more significantly with A (see Fig. 2).

The parameters ϵ_g (the g-boson energy), σ and C_4 are only relevant within the mapped *sdg*-IBM (see, Fig. 4). The values of ϵ_g increase, as functions of A. This reflects, the decreasing trend observed in the $\beta_4^{\rm min}$ values in panels (a), (c) and (e) of Fig. 2. The parameter σ decreases with A, which corresponds to the decrease of both $\beta_4^{\rm min}$ and the ratio $\beta_4^{\rm min}/\beta_2^{\rm min}$. Finally, the increase of C_4 with A reflects the decreasing pattern of $\beta_4^{\rm min}$ with A.

IV. RESULTS OF THE SPECTROSCOPIC CALCULATIONS

A. Excitation energies

The excitation energies of the yrast states with spins in the range $J^\pi = 2^+ - 14^+$, obtained within the *sdg*-IBM model, are plotted in panels (a), (c) and (e) of Fig. 6, as functions of the mass number A. The excitation energies, obtained within the *sd*-IBM model, are shown in panels (b), (d) and (f) of the same figure. One realizes

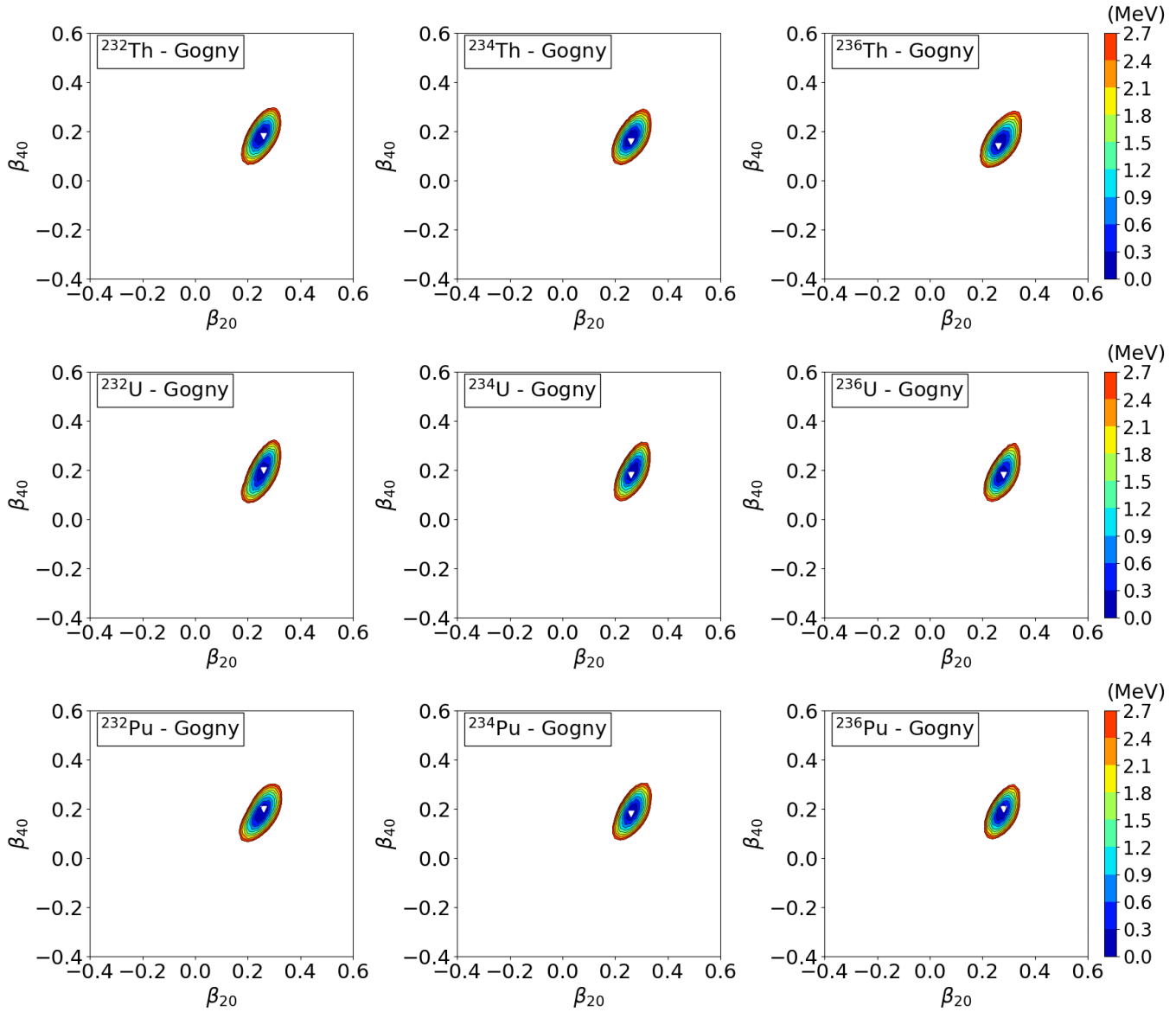


FIG. 1. (Color online) The Gogny-D1S PESs obtained for the nuclei $^{232-236}$Th (first row), $^{232-236}$U (second row) and $^{232-236}$Pu (third row) are plotted as functions of the quadrupole and hexadecapole deformations. The energy difference between neighboring contours is 0.1 MeV. The absolute minima are indicated by open triangles.

that the *sdg*-IBM improves the description of the excitation energies of the high-spin yrast states with $J^+ \geq 10^+$ in almost all of the studied isotopes, as compared with the results obtained within the *sd*-IBM. For the $A = 232$ and 234 isobars, both IBM models tend to overestimate the experimental excitation energies [63] of those states. However, the *sdg*-IBM energies are much closer to the experiment than the *sd*-IBM ones. This reduction of the excitation energies of higher-spin states represents a major outcome of considering the hexadecapole degree of freedom in the *sdg*-IBM calculations.

The g-boson content in a given state can be studied via the expectation value of the g-boson number operator $\langle \hat{n}_g \rangle$ computed with the corresponding *sdg*-IBM wave function. For the yrast states of nuclei with $A = 232 - 236$, we have obtained $0.6 \lesssim \langle \hat{n}_g \rangle \lesssim 0.8$. On the other hand, for those states in nuclei with $A = 238, 240$ we have obtained average values $\langle \hat{n}_g \rangle \approx 0.4$. From these results, we conclude that, to a certain extent, hexadecapole correlations play a role in the yrast bands of actinide nuclei. However, the predicted $\langle \hat{n}_g \rangle$ values are much smaller than the ones found in our previous mapped *sdg*-IBM calculations [37] for rare-earth isotopes, based on the parametrization D1S of the Gogny-EDF.

The improvements in the excitation energies of the yrast states within the *sdg*-IBM, with respect to the *sd*-

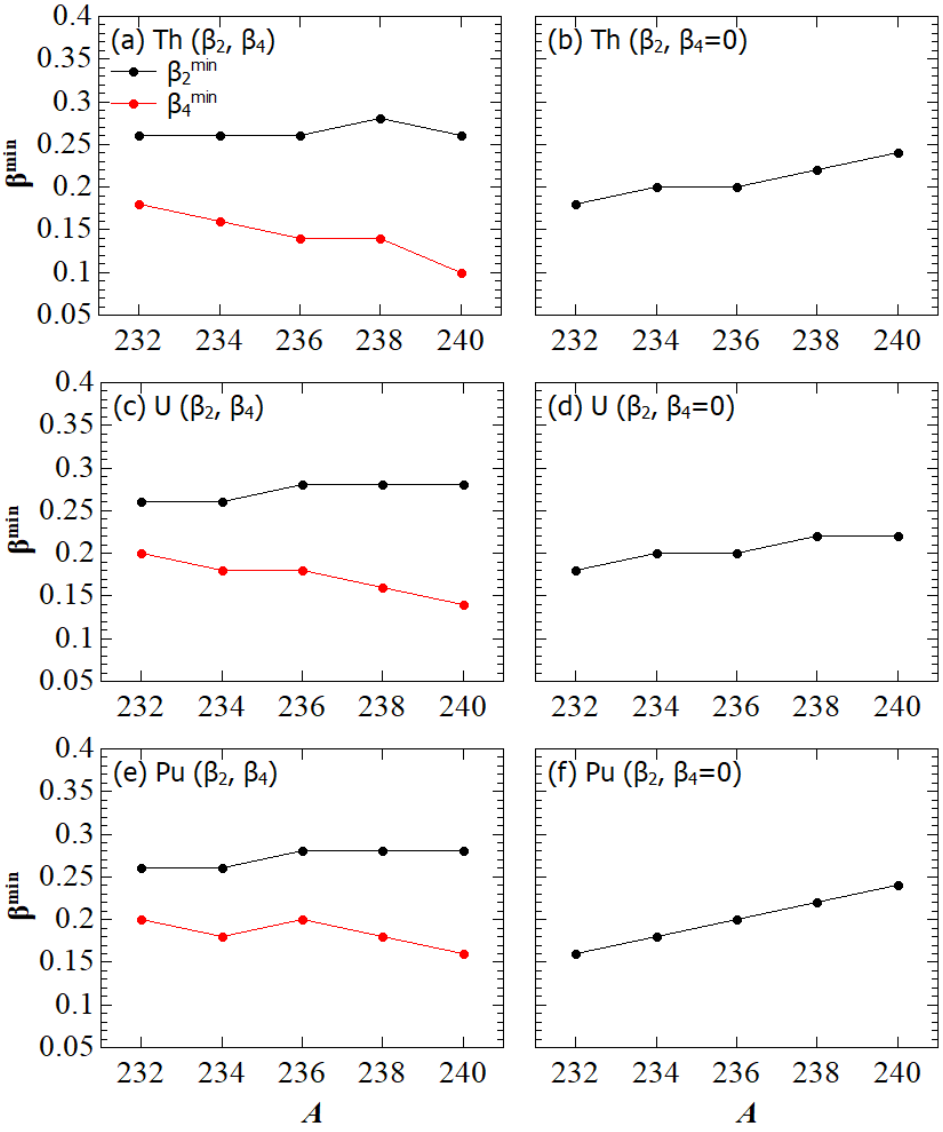


FIG. 2. (Color online) The quadrupole $\beta_2^{\rm min}$ and hexadecapole $\beta_4^{\rm min}$ deformations corresponding to the absolute minima of the Gogny-D1S HFB PESs in Fig. 1 are plotted as functions of the mass number A for the nuclei $^{232-240}$Th [panel (a)], $^{232-240}$U [panel (c)] and $^{232-240}$Pu [panel (e)]. The $\beta_2^{\rm min}$ deformations corresponding to the absolute minima of the PESs in Fig. 1 along the $\beta_4 = 0$ line are depicted in panels (b), (d) and (f).

IBM, are also significantly less pronounced than those obtained for rare-earth nuclei. The inclusion of the g boson in the *sdg*-IBM calculations leads to a lowering in the excitation energies of only ~ 0.3 MeV for the considered actinide nuclei, while for rare-earth nuclei the g boson lowers the energy levels more significantly [37]. This suggests that g bosons have a more limited impact in the higher-spin yrast states of actinides, as compared with rare-earth nuclei. In order to understand the discrepancies it is worth mentioning that the Gogny-D1S PESs for the studied Th, U and Pu nuclei are not as soft along the β_4 direction as those obtained in the rare-earth region [36, 37, 51, 52]

In this study, the nonyrast 0_2^+, 2_3^+ and 4_3^+ states have been considered as members of a possible $K^\pi = 0_2^+$ band according to their level ordering and the dominant $\Delta J = 2$ $E2$ transitions between them. The excitation energies predicted for these states are plotted in Fig. 7, as functions of the mass number A. From the comparison between the *sdg*-IBM results [panels (a), (c) and (e)] with the *sd*-IBM ones [panels (b), (d) and (f)], we conclude that the former model does not provide an improvement with respect to the latter. Note, that for the $A = 238$ isobars the *sdg*-IBM even overestimates the energies of these nonyrast states. It is possible that the use of a more general *sdg*-IBM Hamiltonian [22] could improve the description of the nonyrast states. Nevertheless, one should also keep in mind that the expectation

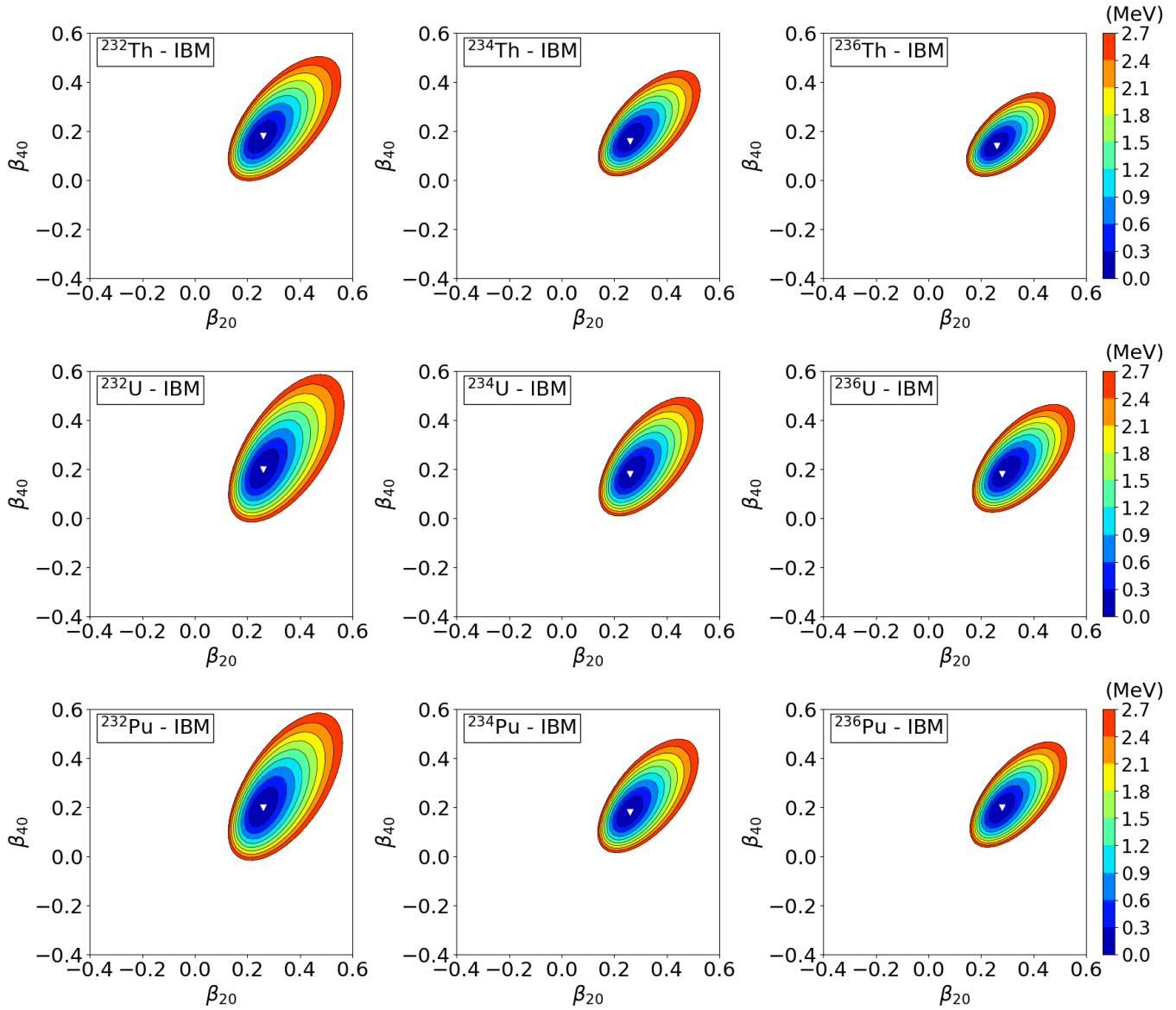


FIG. 3. (Color online) The same as in Fig. 1, but for the mapped *sdg*-IBM PESs of $^{232-236}$Th (first row), $^{232-236}$U (second row) and $^{232-236}$Pu (third row).

values $\langle \hat{n}_g \rangle$ are significantly small, indicating that hexadecapole correlations are rather minor in those states. The study of the hexadecapole effects in actinides with a more general *sdg*-IBM Hamiltonian is out of the scope of this paper. Work along these lines will be reported in future publications.

The excitation energies of the 2_2^+, 3_1^+, and 4_2^+ states, obtained within the *sdg*-IBM model, are plotted in panels (a), (c) and (e) of Fig. 8, as functions of the mass number A. The excitation energies, obtained within the *sd*-IBM model, are shown in panels (b), (d) and (f) of the same figure. Similar to the $K^\pi = 0^+$ excited band, we have associated the 2_2^+, 3_1^+, and 4_2^+ states with a possible $K^\pi = 2^+$ or γ-vibrational band according to the level structure and $E2$ transition patterns. The *sdg*-IBM calculations provide larger excitation energies for the 2_2^+, 3_1^+, and 4_2^+ states than in the *sd*-IBM case and gives a slight improvement in describing the experimental low-lying structure in most of the studied nuclei. The *g*-boson expectation values in these states are $\langle \hat{n}_g \rangle \approx 0.4$, which implies some admixture of hexadecapole components. However, none of the considered mapped IBM models includes triaxiality, i.e., the γ degree of freedom that might improve the description of the γ-band states [31] and therefore it is rather unclear whether the improvement in the comparison with experiment of the members of this band can be ascribed to the hexadecapole collectivity in actinides. Triaxiality can be in-

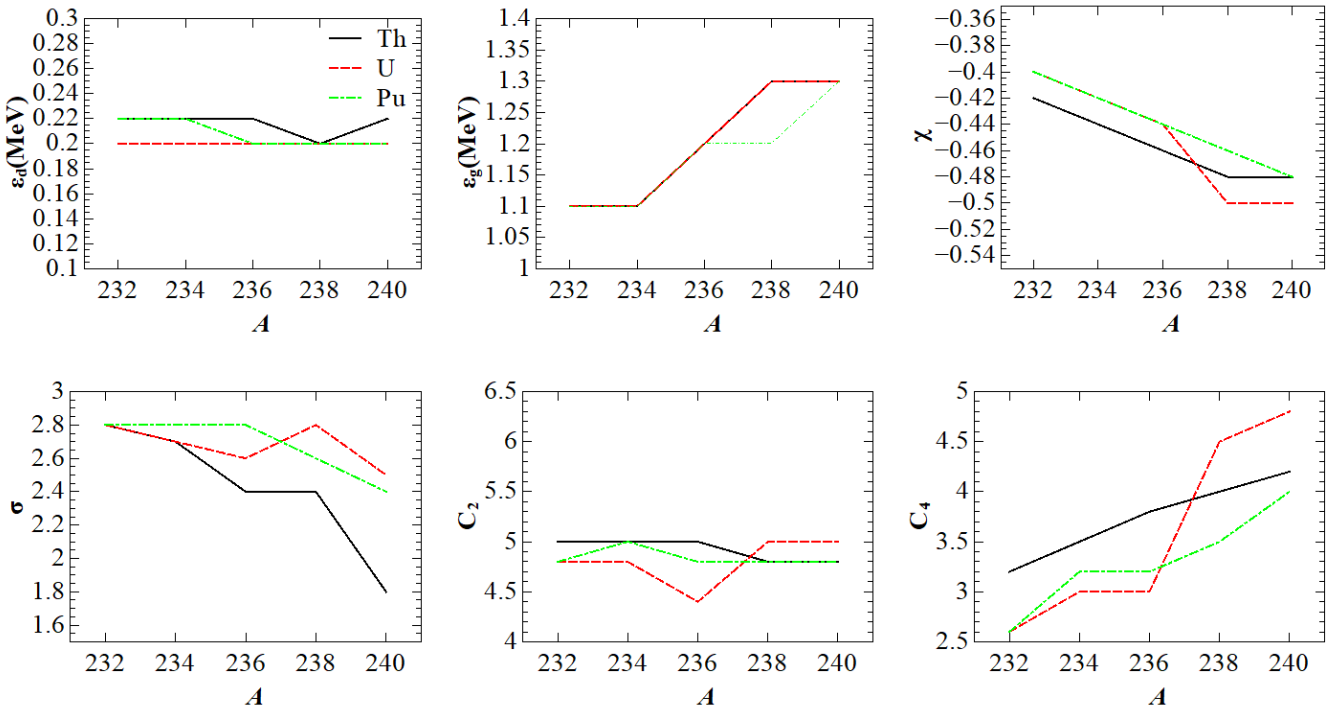


FIG. 4. (Color online) The parameters of the *sdg*-IBM Hamiltonian Eq. (2), obtained for $^{232-240}$Th, $^{232-240}$U and $^{232-240}$Pu, are plotted as functions of the mass number A. For more details, see the main text.

cluded in both the *sdg*-IBM and *sd*-IBM [23], as well as in the SCMF calculations [64–66]. However, such an extension is out of the scope of this work as it would lead to multi-dimensional constrained SCMF calculations, which would significantly complicate the mapping procedure.

B. Transition strengths

1. $E2$ transitions

The $B(E2; J \to J-2)$ transition strengths along the yrast bands of ^{232}Th, ^{236}U and ^{238}U are shown in panels (a), (b) and (c) of Fig. 9. These nuclei have been chosen as illustrative examples for which, experimental data on $E2$ transition strengths for yrast states with $J^\pi = 2^+ - 14^+$ are available. For ^{232}Th, the *sdg*-IBM significantly improves the description of the $E2$ transition strengths over the *sd*-IBM predictions for yrast states with $J^\pi \geqslant 6^+$. However, for both ^{236}U and ^{238}U, an improvement is only obtained in the $J^\pi = 12^+$ and 14^+ states. This reflects that the calculated $\langle \hat{n}_g \rangle$ values are larger in the yrast states of nuclei with $A = 232$ and 234, as compared with the $\langle \hat{n}_g \rangle$ values obtained for $A \geqslant 236$. As a result, the $\sigma(d^\dagger \times \tilde{g} + g^\dagger \times \tilde{g})^{(2)}$ term in the quadrupole operator Eq. (3), which is also part of the $\hat{T}^{(E2)}$ transition operator in Eq. (11), contributes less to the calculated $B(E2)$ strengths along the yrast bands of nuclei with $A \geqslant 236$.

2. Hexadecapole transitions

The $B(E4; 4_n^+ \to 0_1^+)$ $(n = 1, 2, ..., 10)$ values, obtained for the nuclei ^{232}Th, ^{236}U and ^{238}Pu, and within the *sdg*-IBM and *sd*-IBM model spaces are shown in panels (a), (b) and (c) of Fig. 10, as functions of the excitation energies of the 4_n^+ states. Those reduced transition probabilities have been computed using the $E4$ operators (12) for the *sdg*-IBM and (13) for the *sd*-IBM. We have considered the nuclei ^{232}Th, ^{236}U and ^{238}Pu as illustrative examples for which, experimental data for the $B(E4; 4_1^+ \to 0_1^+)$ strengths are available. The *sdg*-IBM and *sd*-IBM $B(E4; 4_1^+ \to 0_1^+)$ values are similar, as the the e_4 effective charges are fitted to reproduce the measured hexadecapole transition strengths. One should note, however, that the e_4 charges in the *sd*-IBM are significantly larger than the *sdg*-IBM ones. This points towards the need of considering g-bosons when computing $B(E4)$ transition strengths. Besides the first 4^+ state, the *sd*-IBM does not predict any strong $E4$ transitions from higher-lying 4^+ states to the ground state. However, the mapped *sdg*-IBM model predicts relatively large $B(E4)$ values for the 4_7^+ state (^{232}Th and ^{238}Pu) or the 4_8^+ state (^{236}U). These 4_7^+ and/or 4_8^+ states can be considered to be bandheads of the $K^\pi = 4^+$ bands since

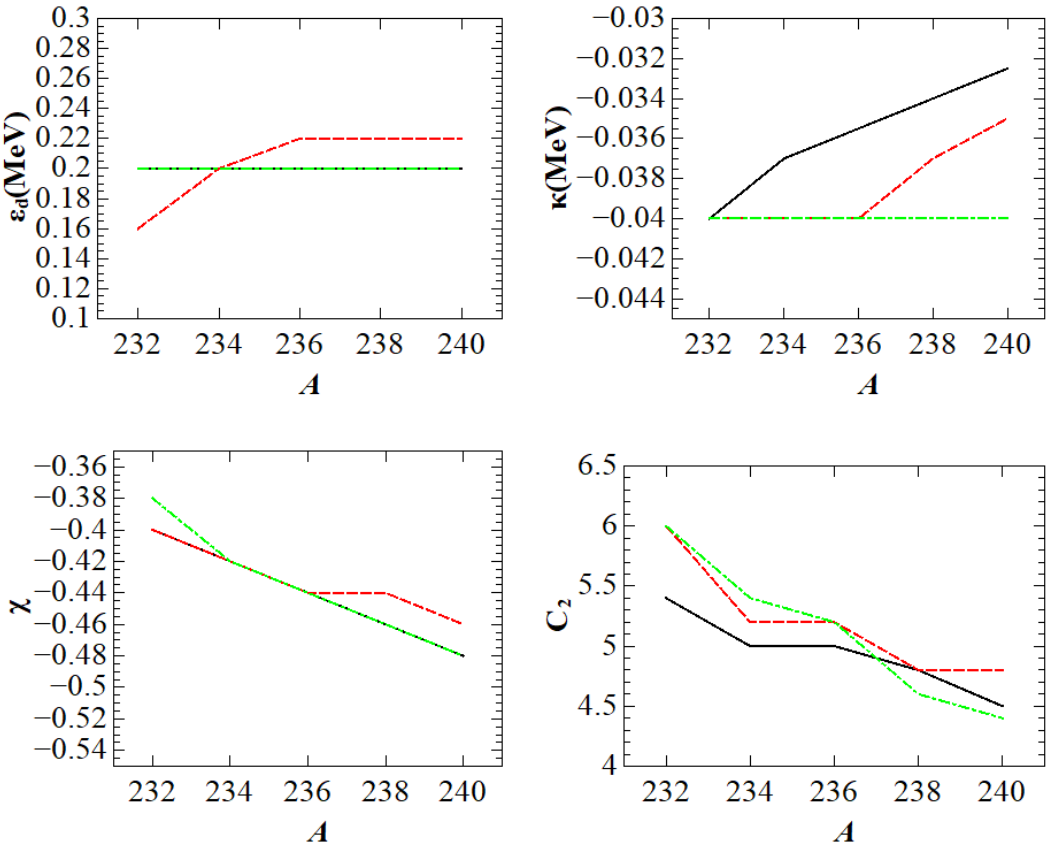


FIG. 5. (Color online) The parameters of the *sd*-IBM Hamiltonian Eq. (8), obtained for $^{232-240}$Th, $^{232-240}$U and $^{232-240}$Pu, are plotted as functions of the mass number A. For more details, see the main text.

for these states, the *sdg*-IBM provides expectation values $\langle \hat{n}_g \rangle \approx 1$.

For some rare-earth nuclei, considered in previous studies [36, 37], the $K^\pi = 4^+$ bandhead 4_3^+ or 4_4^+ states (containing one g boson) were predicted at much lower excitation energies ($E_{\rm exc} < 2.0$ MeV). The fact that the first 4^+ states, in which g bosons are present, are significantly higher in energy in actinides, indicates that hexadecapole correlations are weaker in actinides than in rare-earth nuclei. Therefore, hexadecapole correlations are more significantly overshadowed by quadrupole effects in actinides. There is no experimental information available on the 4_7^+ and 4_8^+ states. Thus, at the present stage, it is not possible to assess the accuracy of the mapped *sdg*-IBM regarding the properties of the 4^+ bands in actinides.

V. SUMMARY

We have carried out a detailed analysis of the quadrupole-hexadecapole collectivity in the even-even actinide nuclei $^{232-240}$Th, $^{232-240}$U, and $^{232-240}$Pu where hexadecapole correlations are expected to play a role in the low-energy dynamics. To this end, we have resorted to the Gogny-D1S HFB framework as initial (fermionic) input followed by the mapped *sdg*-IBM. We have also performed comparisons with results obtained within the simpler mapped *sd*-IBM model in order to understand the role played by the g (hexadecapole) boson.

For most of the studied nuclei, the minima of the (β_2, β_4)-PESs correspond to quadrupole deformations $\beta_2 \approx 0.25$ and hexadecapole deformations $\beta_4 > 0$. The excitation energies of low-lying positive-parity yrast and nonyrast states, obtained via the diagonalization of the *sdg*-IBM Hamiltonian, agree reasonably well with the available experimental data. The results obtained in this work and in the previous study [37] show, that the Gogny-HFB mapped *sdg*-IBM model represents a reasonable starting point to describe the spectroscopic properties of nuclei in different regions of the nuclear chart, such as rare-earth and actinide nuclei for which hexadecapole collectivity plays a role.

We have shown that the mapped *sdg*-IBM model can improve the description of the high-spin yrast states in almost all the studied nuclei, especially those with mass

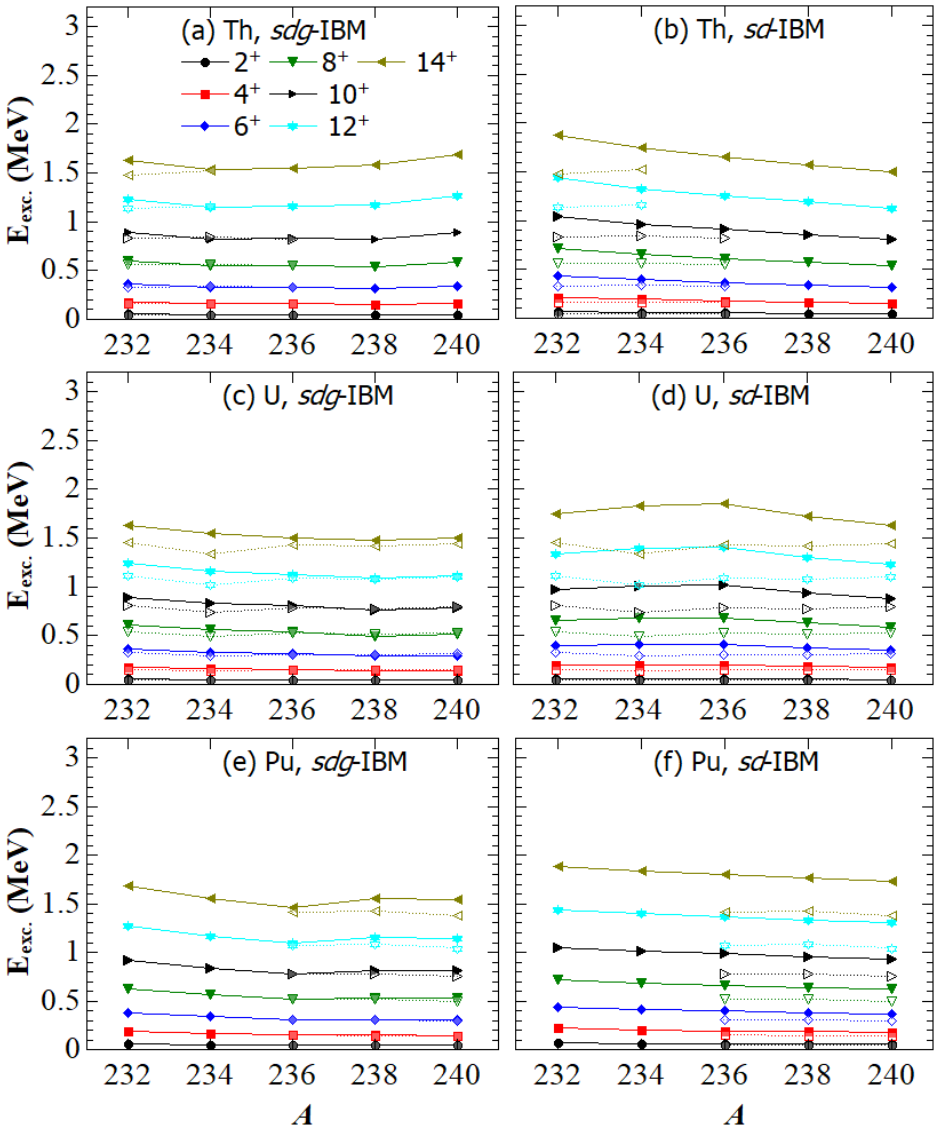


FIG. 6. (Color online) The excitation energies of the yrast band states with spins from $J^\pi = 2^+$ up to $J^\pi = 14^+$ (solid symbols connected by the solid lines), obtained within the *sdg*-IBM model for $^{232-240}$Th, $^{232-240}$U and $^{232-240}$Pu, are plotted in panels (a), (c) and (e) as functions of the mass number A. The corresponding excitation energies, obtained within the *sd*-IBM model, ar shown in panels (b), (d) and (f). The available experimental data, taken from Ref. [63], are depicted as open symbols connected by the dotted lines.

numbers $A = 232$ and 234, for which hexadecapole collectivity is predicted to play a role in the yrast states with even spins $J^\pi \geqslant 10^+$. As compared with the rare-earth region, hexadecapole effects have been found to be rather weak in actinides. For nonyrast states, members of the excited $K^\pi = 0^+$ and $K^\pi = 2^+$ bands, the *sdg*-IBM overestimates the energies of the excited 0^+ states and provides minor improvements in the excitation energies of states in the $K^\pi = 2^+$ band, as compared with the results obtained with the simpler *sd*-IBM Hamiltonian. A more general *sdg*-IBM Hamiltonian could be necessary to better understand how the inclusion of the g-boson affects the energies of the states in the non-yrast bands.

In comparison with the *sd*-IBM, the *sdg*-IBM predicts larger $B(E2)$ values between yrast states, especially for $A = 232$ isobars. This agrees well with the available experimental data and suggests that hexadecapole correlations represent a necessary building block to account for $E2$ transitions in the yrast band of nuclei in this region.

For larger mass numbers, in each isotopic chain, the differences between the *sd*-IBM and *sdg*-IBM $B(E2)$ strengths become smaller, though the effects of hexadecapole collectivity can still be observed in the $J^\pi = 14^+$ states. The *sdg*-IBM model predicts $K^\pi = 4^+$ bands with enhanced $4^+ \rightarrow 0^+$ $E4$ transitions. However, the 4^+_7 and/or 4^+_8 states are predicted at higher excitation ener-

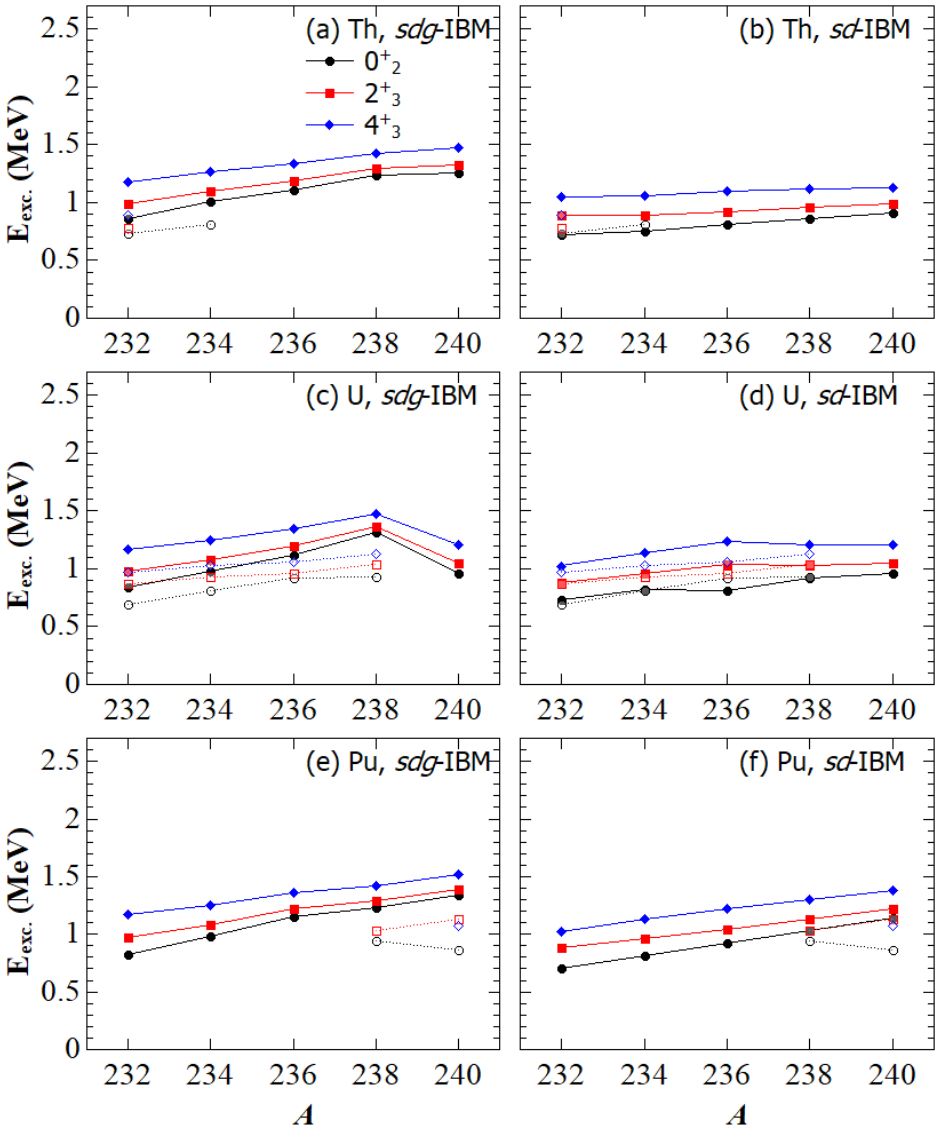


FIG. 7. (Color online) The excitation energies of the 0_2^+, 2_3^+, and 4_3^+ states (solid symbols connected by the solid lines), obtained within the *sdg*-IBM model for $^{232-240}$Th, $^{232-240}$U and $^{232-240}$Pu, are plotted in panels (a), (c) and (e) as functions of the mass number A. The corresponding excitation energies, obtained within the *sd*-IBM model, ar shown in panels (b), (d) and (f). The available experimental data, taken from Ref. [63], are depicted as open symbols connected by the dotted lines.

gies than the $K^\pi = 4^+$ bandheads found for rare-earth nuclei [36, 37]. Experimental information on $E4$ transitions in actinides is required to better understand to which extent the *sdg*-IBM model accounts for the properties of the $K^\pi = 4^+$ bands.

A long list of tasks remains to be done. For example, a potential extension of this study would be to apply the Gogny-HFB mapped *sdg*-IBM framework to regions of the nuclear chart characterized by negative hexadecapole deformations, i.e., square-like shapes, such as W and Os [52] as well as Pt nuclei. Another possible extension of the present work could be the inclusion of both neutron and proton boson degrees of freedom to study the hexadecapole collectivity and mixed-symmetry states of nuclei.

ACKNOWLEDGMENTS

The work of K. Nomura has been supported by JSPS KAKENHI Grant No. JP25K07293. The work of R. Rodríguez-Guzmán is funded by Nazarbayev University under the Faculty Development Competitive Research Grants Program (FDCRGP) for 2025-2027, Grant 040225FD4712. The work of L. M. Robledo is supported by Spanish Agencia Estatal de Investigacion (AEI) of the Ministry of Science and Innovation under Grant No.

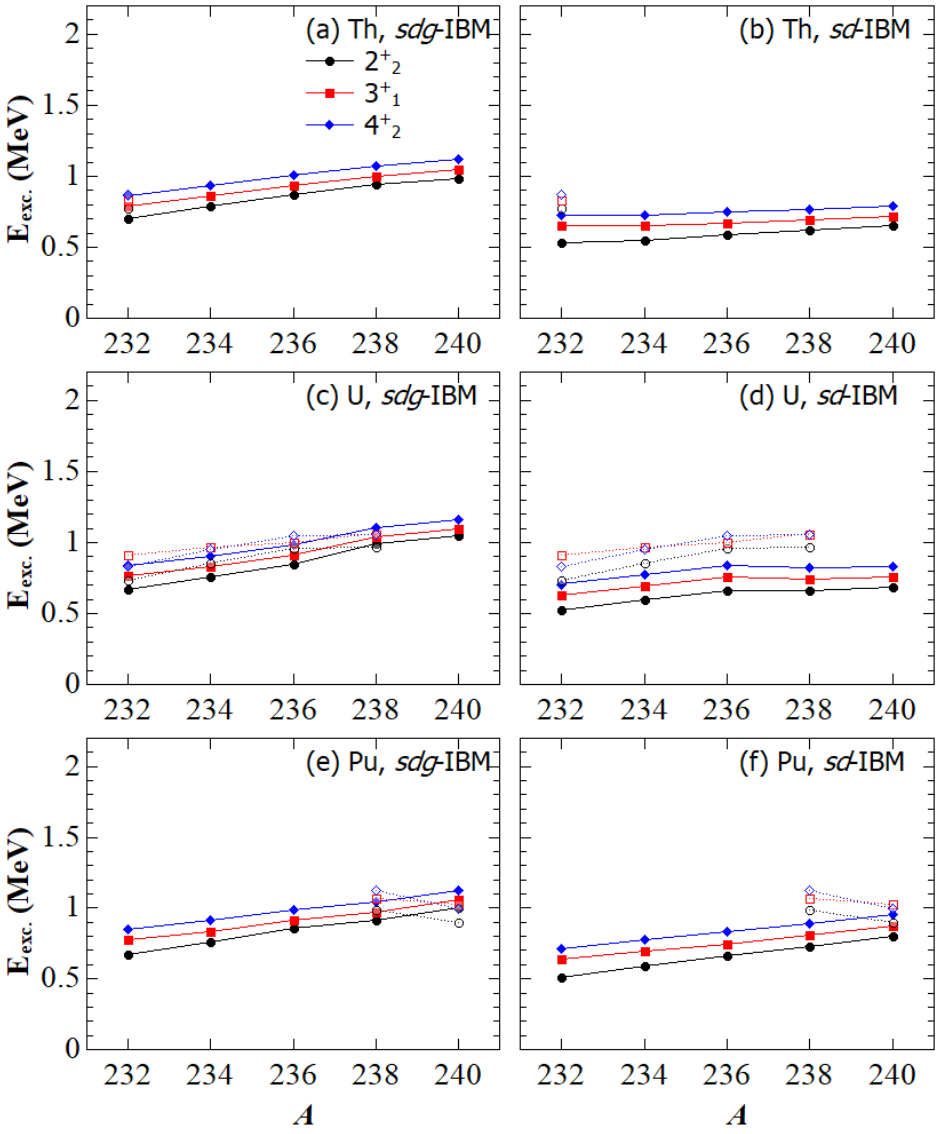


FIG. 8. (Color online) The excitation energies of the 2_2^+, 3_1^+, and 4_2^+ states (solid symbols connected by the solid lines), obtained within the *sdg*-IBM model for $^{232-240}$Th, $^{232-240}$U and $^{232-240}$Pu, are plotted in panels (a), (c) and (e) as functions of the mass number A. The corresponding excitation energies, obtained within the *sd*-IBM model, ar shown in panels (b), (d) and (f). The available experimental data, taken from Ref. [63], are depicted as open symbols connected by the dotted lines.

PID2021-127890NB-I00 and PID2024-159559NB-C21.

[1] A. Bohr and B. R. Mottelson, *Nuclear Structure*, Vol. II (Benjamin, New York, USA, 1975).
[2] Y. Gupta, B. Nayak, U. Garg, K. Hagino, K. Howard, N. Sensharma, M. Şenyiğit, W. Tan, P. O'Malley, M. Smith, R. Gandhi, T. Anderson, R. deBoer, B. Frentz, A. Gyurjinyan, O. Hall, M. Hall, J. Hu, E. Lamere, Q. Liu, A. Long, W. Lu, S. Lyons, K. Ostdiek, C. Seymour, M. Skulski, and B. Vande Kolk, Phys. Lett. B **806**, 135473 (2020).
[3] M. Spieker, S. Agbemava, D. Bazin, S. Biswas, P. Cottle, P. Farris, A. Gade, T. Ginter, S. Giraud, K. Kemper, J. Li, W. Nazarewicz, S. Noji, J. Pereira, L. Riley, M. Smith, D. Weisshaar, and R. Zegers, Physics Letters B **841**, 137932 (2023).
[4] K. A. Erb, J. E. Holden, I. Y. Lee, J. X. Saladin, and T. K. Saylor, Phys. Rev. Lett. **29**, 1010 (1972).
[5] H. Wollersheim and T. W. Elze, Nucl. Phys. A **278**, 87 (1977).

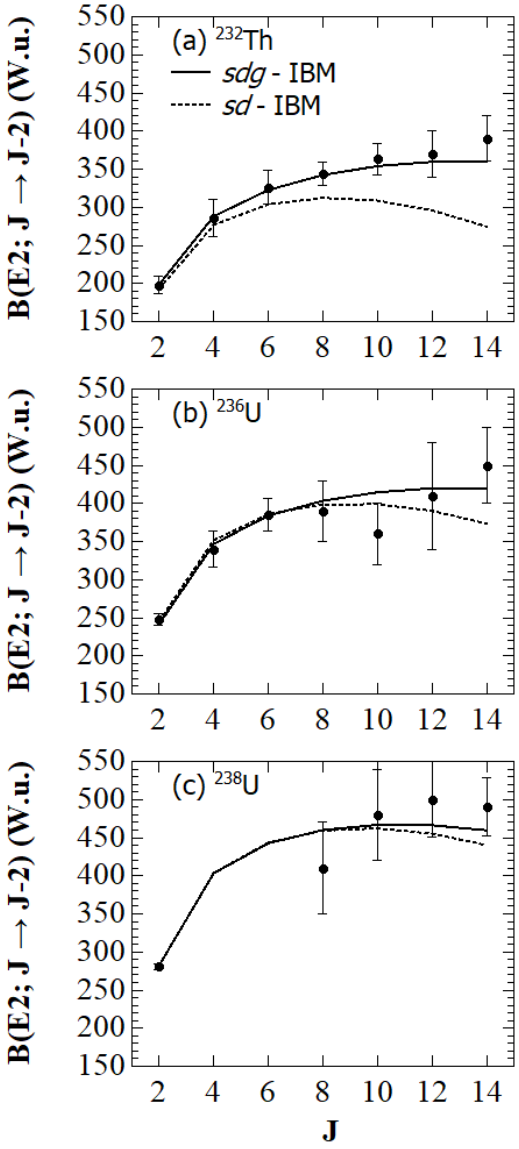


FIG. 9. $B(E2)$ values along the yrast bands of ^{232}Th [panel (a)], ^{236}U [panel (b)] and ^{238}U [panel (c)]. The solid lines represent the results obtained within the *sdg*-IBM, while the dotted lines connect the *sd*-IBM results. The experimental data, represented by the solid circles, are taken from Ref. [63].

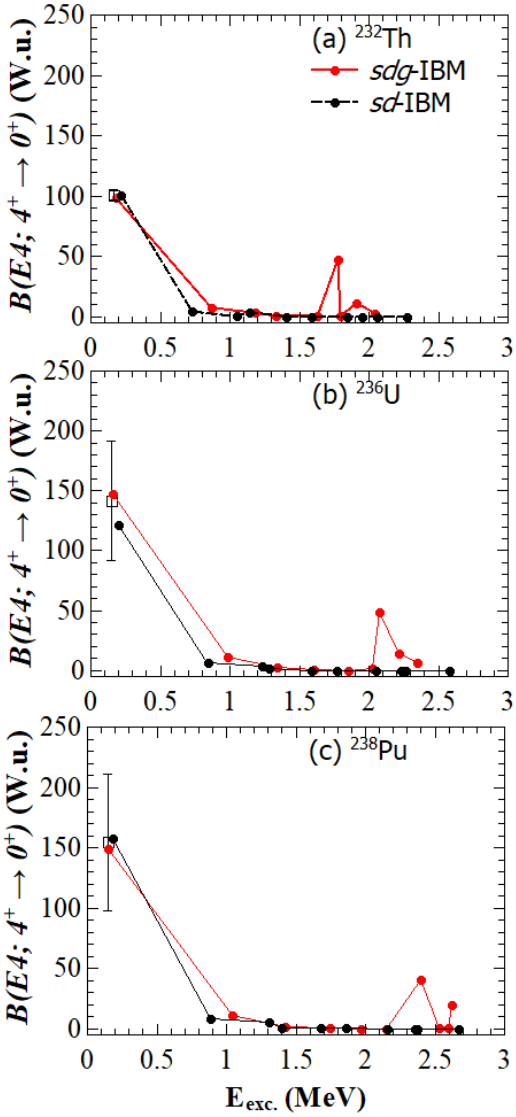


FIG. 10. (Color online) The *sdg*-IBM (red) and *sd*-IBM (black) $B(E4; 4_n^+ \rightarrow 0_1^+)$ $(n = 1, 2, ..., 10)$ values, obtained for the nuclei ^{232}Th [panel (a)], ^{236}U [panel (b)] and ^{238}Pu [panel (c)], are depicted as functions of the excitation energies of the 4_n^+ states. The experimental $B(E4; 4_1^+ \rightarrow 0_1^+)$ data, indicated by open symbols, are taken from Ref. [63].

[6] F. Baker, A. Sethi, V. Penumetcha, G. Emery, W. Jones, M. Grimm, and M. Whiten, Nuclear Physics A **501**, 546 (1989).

[7] A. Sethi, N. M. Hintz, D. N. Mihailidis, A. M. Mack, M. Gazzaly, K. W. Jones, G. Pauletta, L. Santi, and D. Goutte, Phys. Rev. C **44**, 700 (1991).

[8] C. E. Bemis, F. K. McGowan, J. L. C. Ford, W. T. Milner, P. H. Stelson, and R. L. Robinson, Phys. Rev. C **8**, 1466 (1973).

[9] J. D. Zumbro, E. B. Shera, Y. Tanaka, C. E. Bemis, R. A. Naumann, M. V. Hoehn, W. Reuter, and R. M. Steffen, Phys. Rev. Lett. **53**, 1888 (1984).

[10] W. Ryssens, G. Giacalone, B. Schenke, and C. Shen, Phys. Rev. Lett. **130**, 212302 (2023).

[11] H.-j. Xu, J. Zhao, and F. Wang, Phys. Rev. Lett. **132**, 262301 (2024).

[12] B. Schenke, Nuclear Science and Techniques **35**, 115 (2024).

[13] F. Iachello and A. Arima, *The interacting boson model* (Cambridge University Press, Cambridge, 1987).

[14] T. Otsuka, A. Arima, F. Iachello, and I. Talmi, Phys. Lett. B **76**, 139 (1978).

[15] T. Otsuka, A. Arima, and F. Iachello, Nucl. Phys. A **309**, 1 (1978).

[16] R. F. Casten and D. D. Warner, Rev. Mod. Phys. **60**, 389 (1988).
[17] T. Otsuka, Nucl. Phys. A **368**, 244 (1981).
[18] T. Otsuka, A. Arima, and N. Yoshinaga, Phys. Rev. Lett. **48**, 387 (1982).
[19] T. Otsuka and J. N. Ginocchio, Phys. Rev. Lett. **55**, 276 (1985).
[20] T. Otsuka and M. Sugita, Phys. Lett. B **209**, 140 (1988).
[21] Y. D. Devi and V. K. B. Kota, Z. Phys. A **337**, 15 (1990).
[22] S. Kuyucak, Nucl. Phys. A **570**, 187 (1994).
[23] P. Van Isacker, A. Bouldjedri, and S. Zerguine, Nucl. Phys. A **836**, 225 (2010).
[24] K. Nomura, N. Shimizu, and T. Otsuka, Phys. Rev. Lett. **101**, 142501 (2008).
[25] K. Nomura, Eur. Phys. J. A **61**, 139 (2025).
[26] M. Bender, P.-H. Heenen, and P.-G. Reinhard, Rev. Mod. Phys. **75**, 121 (2003).
[27] D. Vretenar, A. V. Afanasjev, G. A. Lalazissis, and P. Ring, Phys. Rep. **409**, 101 (2005).
[28] L. M. Robledo, T. R. Rodríguez, and R. R. Rodríguez-Guzmán, J. Phys. G: Nucl. Part. Phys. **46**, 013001 (2019).
[29] K. Nomura, N. Shimizu, and T. Otsuka, Phys. Rev. C **81**, 044307 (2010).
[30] K. Nomura, T. Otsuka, R. Rodríguez-Guzmán, L. M. Robledo, and P. Sarriguren, Phys. Rev. C **83**, 014309 (2011).
[31] K. Nomura, N. Shimizu, D. Vretenar, T. Nikšić, and T. Otsuka, Phys. Rev. Lett. **108**, 132501 (2012).
[32] K. Nomura, D. Vretenar, and B.-N. Lu, Phys. Rev. C **88**, 021303 (2013).
[33] K. Nomura, D. Vretenar, T. Nikšić, and B.-N. Lu, Phys. Rev. C **89**, 024312 (2014).
[34] K. Nomura, Int. J. Mod. Phys. E **32**, 2340001 (2023).
[35] L. Lotina and K. Nomura, Phys. Rev. C **109**, 034304 (2024).
[36] L. Lotina and K. Nomura, Phys. Rev. C **109**, 044324 (2024).
[37] L. Lotina, K. Nomura, R. Rodríguez-Guzmán, and L. M. Robledo, Phys. Rev. C **111**, 024301 (2025).
[38] D. Gogny, Nuclear Physics A **237**, 399 (1975).
[39] J. Berger, M. Girod, and D. Gogny, Nuclear Physics A **428**, 23 (1984).
[40] S. Hilaire and M. Girod, Eur. Phys. J. A **33**, 237 (2007).
[41] K. Nomura, T. Otsuka, R. Rodríguez-Guzmán, L. M. Robledo, P. Sarriguren, P. H. Regan, P. D. Stevenson, and Z. Podolyák, Phys. Rev. C **83**, 054303 (2011).
[42] K. Nomura, T. Otsuka, R. Rodríguez-Guzmán, L. M. Robledo, and P. Sarriguren, Phys. Rev. C **84**, 054316 (2011).
[43] K. Nomura, R. Rodríguez-Guzmán, and L. M. Robledo, Phys. Rev. C **95**, 064310 (2017).
[44] K. Nomura, R. Rodríguez-Guzmán, Y. M. Humadi, L. M. Robledo, and H. Abusara, Phys. Rev. C **96**, 034310 (2017).
[45] K. Nomura, R. Rodríguez-Guzmán, and L. M. Robledo, Phys. Rev. C **92**, 014312 (2015).
[46] K. Nomura, R. Rodríguez-Guzmán, Y. M. Humadi, L. M. Robledo, and J. E. García-Ramos, Phys. Rev. C **102**, 064326 (2020).
[47] K. Nomura, R. Rodríguez-Guzmán, L. Robledo, and J. García-Ramos, Phys. Rev. C **103**, 044311 (2021).
[48] K. Nomura, R. Rodríguez-Guzmán, L. M. Robledo, J. E. García-Ramos, and N. C. Hernández, Phys. Rev. C **104**, 044324 (2021).
[49] K. Nomura, R. Rodríguez-Guzmán, and L. M. Robledo, Phys. Rev. C **104**, 054320 (2021).
[50] C. V. N. Kumar and L. M. Robledo, Phys. Rev. C **108**, 034312 (2023).
[51] R. Rodríguez-Guzmán and L. M. Robledo, Phys. Rev. C **111**, 024304 (2025).
[52] R. Rodríguez-Guzmán and L. M. Robledo, The European Physical Journal A **61**, 166 (2025).
[53] P. Ring and P. Schuck, *The Nuclear Many-Body Problem* (Springer-Verlag, Berlin, 1980).
[54] T. Nikšić, D. Vretenar, and P. Ring, Prog. Part. Nucl. Phys. **66**, 519 (2011).
[55] P. A. Butler and W. Nazarewicz, Rev. Mod. Phys. **68**, 349 (1996).
[56] P. A. Butler, J. Phys. G: Nucl. Part. Phys. **43**, 073002 (2016).
[57] M. Spieker, D. Bucurescu, J. Endres, T. Faestermann, R. Hertenberger, S. Pascu, S. Skalacki, S. Weber, H.-F. Wirth, N.-V. Zamfir, and A. Zilges, Phys. Rev. C **88**, 041303 (2013).
[58] M. Spieker, S. Pascu, D. Bucurescu, T. M. Shneidman, T. Faestermann, R. Hertenberger, H.-F. Wirth, N.-V. Zamfir, and A. Zilges, Phys. Rev. C **97**, 064319 (2018).
[59] V. K. B. Kota, J. V. der Jeugt, H. E. D. Meyer, and G. V. Berghe, Journal of Mathematical Physics **28**, 1644 (1987).
[60] J. N. Ginocchio and M. W. Kirson, Nucl. Phys. A **350**, 31 (1980).
[61] A. E. L. Dieperink, O. Scholten, and F. Iachello, Phys. Rev. Lett. **44**, 1747 (1980).
[62] S. Heinze, computer program ARBMODEL, University of Cologne (2008).
[63] Brookhaven National Nuclear Data Center, `http://www.nndc.bnl.gov`.
[64] R. Rodríguez-Guzmán, P. Sarriguren, L. M. Robledo, and J. E. García-Ramos, Phys. Rev. C **81**, 024310 (2010).
[65] L. M. Robledo, R. R. Rodríguez-Guzmán, and P. Sarriguren, Phys. Rev. C **78**, 034314 (2008).
[66] B.-N. Lu, J. Zhao, E.-G. Zhao, and S.-G. Zhou, Phys. Rev. C **89**, 014323 (2014).